Ocean Engineering 195 (2020) 106706

Contents lists available at ScienceDirect

Ocean Engineering

journal homepage: www.elsevier.com/locate/oceaneng

Development of a numerical marine weather routing system for coastal and marginal seas using regional oceanic and atmospheric simulations

Kenta Kurosawa [a,b,*], Yusuke Uchiyama [c,d], Taichi Kosako [d]

[a] RIKEN Center for Computational Science, Kobe, Japan
[b] Department of Atmospheric and Oceanic Science, University of Maryland, College Park, MD, USA
[c] Department of Civil Engineering, Kobe University, Kobe, Japan
[d] Coastal and Estuarine Environment Department, Port and Airport Research Institute, Yokosuka, Japan

ARTICLE INFO

Keywords:
Weather routing
A-star algorithm
ROMS
Kuroshio
Optimal route
Numerical simulations

ABSTRACT

The primary objective of this study is to develop a new weather routing system for vessel navigation in coastal and marginal seas based on the A-star algorithm. The cost function inherent in the original A-star algorithm is modified to account for oceanic and atmospheric conditions around the vessel of interest. Three options are introduced to search for optimal paths with the shortest travel distance, shortest travel time, and minimal fuel consumption. An avoidance algorithm for unsafe conditions is further incorporated to exempt any arbitrary area from the navigation solution. Furthermore, a compact ocean circulation model based on the Regional Ocean Modeling System executable on typical laptop PCs is configured for a vessel-borne weather routing system; the system is successfully applied to evaluate the optimal vessel paths in the Seto Inland Sea, where high-frequency tidal currents modified by complex topography make it essential to alter the vessel's speed.

1. Introduction

Reduction of carbon dioxide (CO_2) emission has been a long-standing issue for mediating global warming. Among others, fuel efficiency in ship navigation is recognized as a fundamental factor that must be remedied. Buhaug et al. (2009) presents that the proportion of CO_2 from ship emissions in 2007 was estimated to be 1,046 million tons, accounting for 3.3% of the global CO_2 emission during that year. For economical operation in marine logistics, optimal routing to determine on-time or shortest cruising path is indispensable. In particular, finding the shortest path is often more essential to immediate excursions for fishing, rescues, and leaked contaminants, and to provide urgent evacuation from coastal disasters such as tsunamis and storms. However, vessel navigation is affected significantly by ambient oceanic and atmospheric conditions that restrict the optimal paths. For instance, opposing oceanic currents reduce the vessel's relative speed or increase fuel consumption, whichever the operator cares for more seriously (Trodden et al., 2015; Bouman et al., 2017). Therefore, weather routing (hereinafter denoted as WR), in which surrounding oceanic and atmospheric conditions are taken into account in navigation, is highly desirable for desirable vessel navigation.

In general, WR determines the optimal route by considering many factors such as weather and oceanic conditions, characteristics of ships, and areas of territorial waters (Sen and Padhy, 2010; Tsou and Cheng, 2013). WR differs from automotive navigation systems in many aspects. For example, while automotive navigation systems usually consider only traffic congestion and negotiable roads, WR must account for natural phenomena such as oceanic currents, wind speeds, and wave heights. Moreover, in the open ocean, there are very few obstacles except islands and territorial waters in contrast to the land. Hence, because WR must deal with an infinite number of routes consisting of vast numbers of links and nodes but with fewer guideposts to find the optimal route, its computational cost becomes drastically more expensive than that for automobile navigation. Furthermore, it is necessary to design WR algorithms properly not only for the shortest route (Efentakis et al., 2011) but also for the safest route (Kosmas and Vlachos, 2012), the minimum fuel route (Jung and Rhyu, 1999; Papanikolaou et al., 2016), and the combinations of these factors (Szlapczynska, 2007; Andersson, 2015). Therefore, previous studies have attempted to develop path-finding algorithms while minimizing the computational cost of WR.

One of the more popular methods for finding an optimal route for WR is the isochrone method proposed by Journée and Meijers (1980). Although this method has been used for decades because of its simplicity, the isochrones have to be manually determined *a priori*.

* Corresponding author. RIKEN Center for Computational Science (R-CCS), 7-1-26 Minatojima-minami-machi, Chuo-ku, Kobe, Hyogo, 650-0047, Japan.
E-mail address: kkurosaw@umd.edu (K. Kurosawa).

https://doi.org/10.1016/j.oceaneng.2019.106706
Received 3 July 2019; Received in revised form 30 September 2019; Accepted 7 November 2019
Available online 19 November 2019

Hagiwara (1989) improved the isochrone method to be suitable for computers by implementing an automated isochrone detection algorithm. However, the isochrone method occasionally generates so-called "isochrone loops" making path finding impossible, and failing to avoid crossing lands. Hence, De Wit (1990) and Calvert et al. (1991) introduced dynamic programming, which uses a grid system that divides a possible sailing region into several cells where each crossing point of a cell boundary is used as a waypoint candidate. Some studies have made efforts to conduct a series of detailed investigations to reduce the navigators' workload by using a dynamic programming method for grid size setting and design of the WR system (Wei and Zhou, 2012; Kim and Lee, 2018). Although these methods have been developed elaborately to account for oceanic and atmospheric conditions as much as possible, their main drawbacks are computational inefficiency caused by a large number of nodes, a requirement for large storage space, inflexibility, and slow computational speed.

With a gridded sea area, Dijkstra's algorithm (Dijkstra, 1959) in graph theory is well known to be practical for ship navigation. The algorithm begins at a specific node and extends outwards to calculate the shortest path between any two vertices in a weighted graph (Fig. 1a). Because the algorithm requires searches for all the nodes between the origin and destination, it is computationally very expensive if the sea area of interest is gridded at fine lateral spacing. By contrast, the A-star algorithm (Hart et al., 1968), a modified method of Dijkstra's algorithm, uses heuristics by introducing a cost function for determining the shortest path to the destination (Fig. 1b). As compared to the original Dijkstra's algorithm, the A-star algorithm enables us to significantly reduce computational cost to determine the optimal route by preferentially searching for the adjacent links and nodes pointing to the destination. As illustrated above, there are a substantial number of studies and algorithms for WR with some comparative assessments among the methods (e.g., Roh, 2013; Walther et al., 2016), but the definitive algorithm suitable for WR has not yet been confirmed.

In this study, our first objective is to propose a new marine WR system based upon the A-star algorithm for determining the shortest path to the destination. A cost function is additionally introduced to account for oceanic and atmospheric conditions around the vessel of interest, combined with the heuristic function defined in the original A-star algorithm. In other words, this study proposes to modify the cost function so that three options are considered to search for the optimal paths: shortest travel distance, shortest travel time, and minimal fuel consumption.

Furthermore, most of previous WR studies have focused on ocean-going vessels and ocean liners that cruise mostly on the open ocean. Their routing algorithms are mainly for long voyages where a wide range of route choices is possible. Nevertheless, it is difficult to apply such algorithms directly for vessels sailing on coastal and marginal seas (Smierzchalski and Michalewicz, 2000; Chen et al., 2013). The primary reason is complexity of weather and oceanic conditions as well as coastline topography, all of which are necessary for coastal WR. Thus, there is room for improvement on WR in such areas. One of the more significant issues arises from a poor resolution of the oceanic and atmospheric information released from agencies concerned. In general, these products have quite large spatial resolutions and large update intervals. For example, a regional oceanic reanalysis/forecast product, the Japan Coastal Ocean Prediction Experiment (JCOPE2; Miyazawa et al., 2009) of the Japan Agency for Marine-earth Science and Technology (JAMSTEC), provides daily-averaged data at a lateral grid spacing of about 10 km. This resolution is not sufficient in crowded harbors and bays, where detailed navigation is crucial, because high-frequency variability such as tidal currents characterize the ambient oceanic condition most prominently. Moreover, data retrieval prior to departure and subsequent onboard predictions are occasionally indispensable because ample data retrieval through communications satellites during the voyage may not be feasible. Therefore, this study also configures a compact and computationally efficient regional ocean model executable on typical laptop PCs aiming at a vessel-borne weather routing system for suboptimal availability of weather and oceanic reanalysis/prediction. The model is coupled with the WR system based on the A-star algorithm to evaluate the optimal vessel paths. Our test bed is the Seto Inland Sea (hereafter SIS), Japan, filled with an enormous number of commercial carriers and small fishery and pleasure boats. In the SIS, the high-frequency tidal currents modified by complex topography are substantial to alter the vessel's speed for optimal navigation.

Therefore, this study aims to achieve the following.

1. Develop a new WR system based on the A-star algorithm, which calculates an optimal route with consideration of oceanic and atmospheric conditions, having capabilities of rerouting and avoidance functions for more accurate and safer navigation;
2. Assess the efficiency of the newly developed WR system by applying it to several scenarios including evacuation from a migrating typhoon; and
3. Configure a compact regional ocean circulation model executable on typical laptop PCs aiming at a vessel-borne WR.

This paper is organized as follows. Section 2 describes the proposed algorithms for the WR system. The configurations of the numerical models are given in Section 3. The experimental results with the new WR algorithm are presented and discussed in Section 4. Finally, summaries of this study are presented in Section 5.

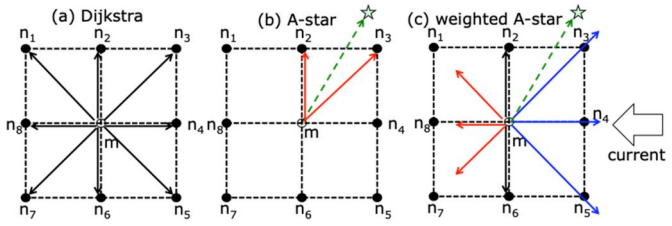

Fig. 1. Schematic diagrams of searching algorithms of (a) original Dijkstra's method, (b) original A-star method, and (c) proposed new weighted A-star method. The start node denoted by m at the center seeks the optimal route among the eight neighboring candidate nodes $n_1 - n_8$ during the first iteration. Lengths of the arrows denote relative magnitudes of the cost χ. The star marks are the final destinations located in the far field with heuristics h_m at m. The A-star algorithm in (b) may preferentially search only n_2 and n_3 because of the shortest heuristics of h_{n2} or h_{n3}. The ambient current approaches from the east to alter the cost χ in (c), either to shorten (red arrows) or to elongate (blue arrows) the effective distance. (For interpretation of the references to color in this figure legend, the reader is referred to the Web version of this article).

2. Weather routing algorithms

2.1. A-star and Dijkstra's algorithms

In this study, a new marine ship routing system is proposed based on the A-star algorithm (Hart et al., 1968, Fig. 1b). This algorithm finds the shortest path to the destination using inter-node traveling cost (hereafter χ) and a heuristic function (hereafter h). The heuristic function h is defined as the shortest path from each node to the final destination node determined *a priori* to minimize the cost χ to search neighboring nodes for candidates comprising the optimal path. Hence, the A-star algorithm enables us to significantly reduce computational time needed to determine the optimal route by using h as the "guidepost." If h is set at zero, the A-star algorithm simply reverts back to Dijkstra's algorithm (Fig. 1a).

Fig. 2 compares the efficiency of the Dijkstra's algorithm and the A-star algorithm in searching for the shortest path from the origin to the destination by illustrating the estimated shortest paths and the number of searches at every grid point. Even if no obstacles exist on the possible path (Fig. 2a and b), Dijkstra's algorithm with $h = 0$ searched all the grid

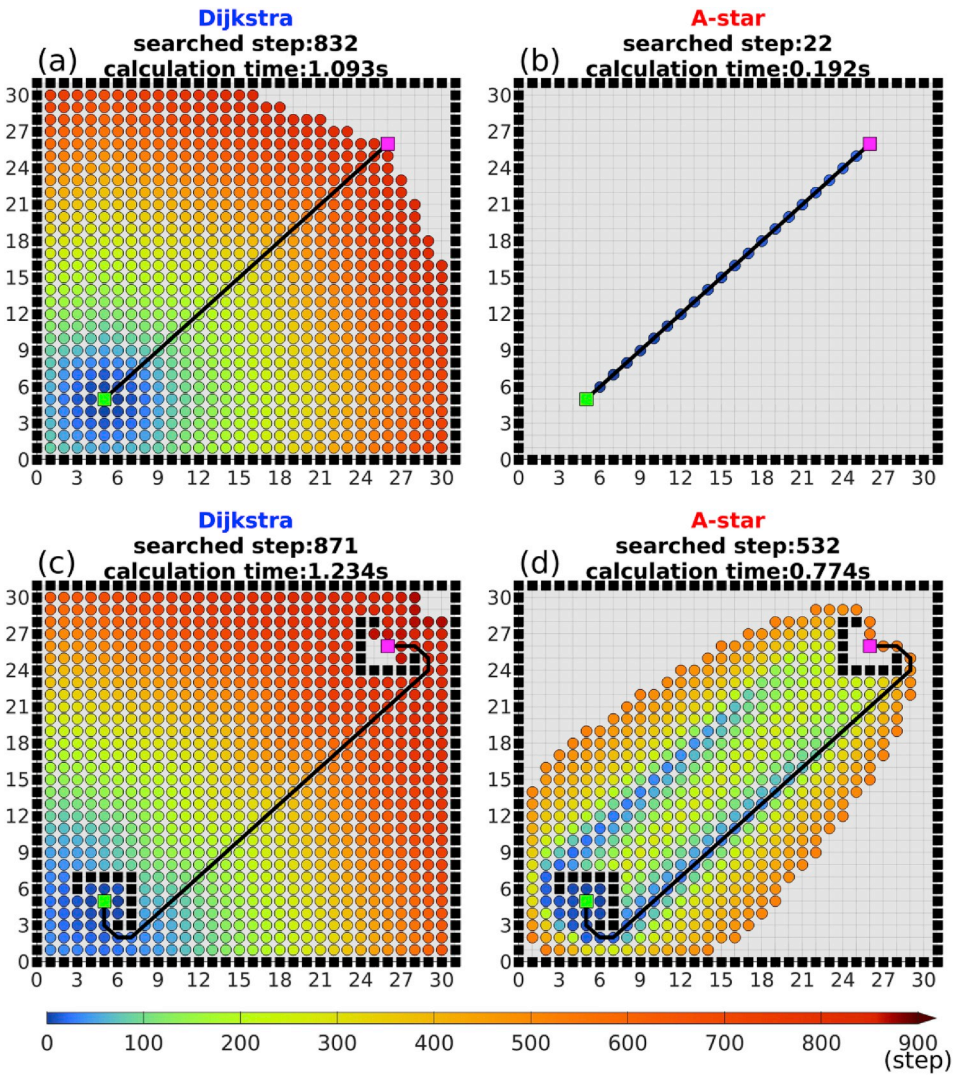

Fig. 2. Schematic plots of Dijkstra's algorithm and the A-star algorithm examples. The black curves are the shortest routes determined by Dijkstra's algorithm (a and c) and the A-star algorithm (b and d). The green and magenta squares are the origin and destination, respectively. The circles indicate that the grid points are searched during iteration with colors indicating number of the searched steps. The black squares are obstacles excluded from the graph searches. (For interpretation of the references to color in this figure legend, the reader is referred to the Web version of this article).

points between the origin and the destination (Fig. 2a). On the other hand, the A-star algorithm successfully finds the shortest path without any unnecessary searches (Fig. 2b) that ensures significant improvement in computational efficiency. If we place obstacles representing breakwaters of port facilities near the origin and destination, the two algorithms detect the same optimal routes, whereas the A-star algorithm requires fewer computational steps and searched grid points than Dijkstra's algorithm (Fig. 2c and d). Therefore, the A-star algorithm significantly reduces search cost to find the shortest path without losing precision as compared to Dijkstra's algorithm.

2.2. Three options useful for marine WR

The traveling cost χ and heuristics h inherent in the original A-star algorithm are designed with Euclidean distances. The optimal route is determined by minimizing the sum of the cost χ and the heuristics h, such that the optimal route follows the paths of shortest Euclidean distance. In this study, we incorporate the great-circular distance (hereinafter, simply referred to as an arc length) to χ and h, and the effect of oceanic current and other factors to χ. The first modification has usually been done in other marine WR algorithms. The arc length L between two locations at (latitude φ_1, longitude λ_1) and (φ_2, λ_2) on the globe with a diameter of R may be approximated as

$$L = R\,acos[sin\varphi_1 sin\varphi_2 + cos\varphi_1 cos\varphi_2 cos(\lambda_1 - \lambda_2)]. \quad (1)$$

Thus, in the shortest travel distance method, the optimal route is searched without considering oceanic currents, so the inter-node traveling cost function from node m to node n ($\chi_{n|m}$) is defined merely as

$$\chi_{n|m} = \boldsymbol{L}, \quad (2)$$

where L is the arc length between nodes n and m as computed by Eq. (1).

In the second modification, we consider a weight on the cost χ by reflecting changes of the vessel's relative velocity to the local background currents as changes of an effective inter-node traveling distance (Fig. 1c); i.e., we assume that the traveling distance is either shortened or elongated due to background current velocity. If a vessel is sailing on still water at V_o but the ocean moves at V_i due to currents, then the resultant absolute vessel speed is V_o+V_i. Accordingly, $\chi_{n|m}$ is modified as:

$$\chi_{n|m} = \frac{V_o}{V_o + V_i} L. \quad (3)$$

If the ambient current direction coincides with the vessel's traveling direction, i.e., $V_o+V_i > V_o$, then the weighted $\chi_{n|m} < L$, so that the navigator may favor sailing the vessel in this direction for the shorter travel time.

In contrast, if the underlying current is in the same direction as the vessel, then the vessel can decelerate its relative speed to V_o-V_i to keep the absolute vessel speed unchanged to reduce fuel consumption. According to previous studies (e.g., Lu et al., 2015; Bialystocki and

Konovessis, 2016), fuel consumption of vessels is quadratically proportional to the relative vessel speed. Hence, we introduce another modification for the minimal fuel consumption method, in which

$$\chi_{n|m} = L\left(\frac{V_o - V_i}{V_o}\right)^2. \quad (4)$$

As a result, three options are introduced to search for the optimum paths with the shortest travel distance: (1) without considering oceanic currents, (2) minimizing travel time while maintaining a constant propeller speed, and (3) minimizing fuel consumption by preserving a constant vessel speed affected by oceanic currents while altering propeller speed. Although the first method corresponds to the original A-star algorithm, the latter two methods rely on the weighted cost function χ modified by oceanic and atmospheric conditions.

In addition, a rerouting function is also implemented, as well as an avoidance function, for arbitrary areas where there are waves, wind, chemicals, and any conditions that are undesirable for navigation. The former is achieved simply by re-computation of the optimal route whenever it is demanded upon updates of oceanic, atmospheric, or vessel conditions. The latter is viable by removing the nodes that the vessel should avoid from WR computations.

3. Regional ocean circulation models

The ocean model we use in this study is the Regional Oceanic Modeling System (ROMS; Shchepetkin and McWilliams, 2005, 2008), a terrain-following, 3D primitive equation ocean circulation model with the hydrostatic and Boussinesq approximations. The following subsections describe the model configurations used for the WR experiments to validate and evaluate the proposed algorithms.

3.1. Northwestern Pacific Ocean model

The first configuration used in this study is the Northwestern Pacific Ocean downscaling ROMS model (hereinafter NWPO; Fig. 3 and Table 1) developed in Tada et al. (2018). The daily averaged JCOPE2 reanalysis with a lateral grid spacing of ~10 km is used as the initial and open boundary conditions. The atmospheric conditions are imposed by using the Grid-Point-Value MesoScale Model (GPV-MSM), a high-resolution atmospheric reanalysis product published by the Japan Meteorological Agency (JMA). The NWPO model domain extends horizontally 1,840 km × 1,440 km with a lateral grid spacing of 2 km to encompass a sufficiently wide area that includes the Kuroshio path and the track of Typhoon 201418 (Phanfone). Temperature-salinity nudging (T-S nudging; Marchesiello et al., 2003; Uchiyama et al., 2018a) with a weak nudging inverse time scale of 1/20 d^{-1} is applied towards the 10-day averaged JCOPE2 3D temperature and salinity fields to assure long-term reproducibility of the Kuroshio path. This model was extensively validated to show good agreement with satellite and *in situ* observations in Tada et al. (2018). The NWPO model is used for testing graph-search problems in consideration of the Kuroshio path and rerouting and avoidance functions under a typhoon condition in Sections 4.1 and 4.2.

Table 1
Model configurations.

Models	NWPO	Seto-2km	Seto-600m
Computational period	1/1/2013 - 12/31/2014	1/1/2013 - 2/28/2013	9/1/2006 - 11/9/2015
Grid cells	800×480 (×32 vertical layers)	224×192 (×20 layers)	800×480 (×32 layers)
Horizontal grid resolution	2.0 km	2.0 km	600 m
Baroclinic time step	120 s	120 s	30 s
Surface wind stress	JMA-MSM (hourly)	JMA-MSM (hourly)	JMA-MSM (two hourly)
Surface flux	COAMPS bulk formula	COADS (monthly clim.)	COAMPS bulk formula
Boundary/ Initial condition	JCOPE2 (daily)	JCOPE2 (daily)	Parent ROMS-L1 (daily)
T-S nudging	JCOPE2 (10-day averaged)	None	None
Topography	SRTM30+JEGG500	SRTM30+JEGG500	SRTM30+JEGG500
Major river discharges	Japan River Association (monthly climatology)	None	Japan River Association (monthly clim.)
Tide	None	TPXO7.0	TPXO7.0

3.2. Compact ocean model

We configure a compact ocean model for the SIS (hereinafter Seto-2km; Fig. 3) that is sufficiently suited to execute on laptop computers or even on tablets and smartphones for a vessel-borne, quasi-standalone WR system. The model is again based on ROMS and designed to encompass the SIS and the Kuroshio with a horizontal grid spacing of 2 km. A one-way offline nesting is employed from the assimilative JCOPE2 oceanic reanalysis. Ten tidal constituents from the TPXO7.0 global tidal reanalysis (Egbert et al., 1994; Egbert and Erofeeva, 2002) are additionally imposed on the open boundaries to account for substantial tidal currents in the SIS. Other numerical conditions are listed in

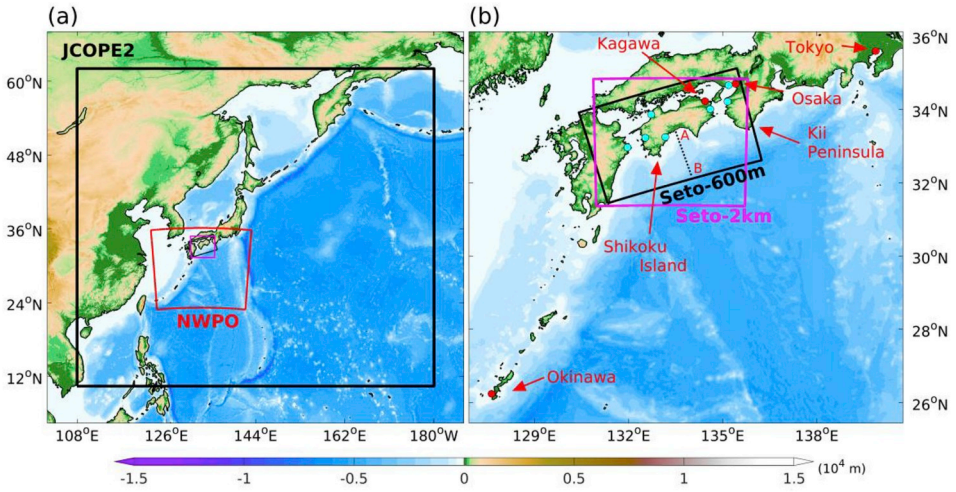

Fig. 3. Model domains with bathymetry in color. (a) Black box: JCOPE2, red box: NWPO model, and magenta box: Seto-2km model (also shown in b), (b) black box: Seto-600m model. The black dotted line in (b) identifies the transect A-B for the cross-sectional plots in Fig. 5. The cyan circles depict the locations of tide gauge stations used for the harmonic analysis in Fig. 7. (For interpretation of the references to color in this figure legend, the reader is referred to the Web version of this article).

Table 1. By reducing horizontal and vertical resolutions, omitting river inflows, and simplifying the surface flux estimation without losing the required accuracy, the model can compute 3D oceanic currents and density field for one calendar day in approximately 4 min using a typical laptop PC. In the following analyses, the Seto-2km ROMS model runs for a two-month period including the initial spin-up of one month.

3.3. Validation of the compact ocean model

The results of the Seto-2km model are compared with those of another higher-resolution SIS model developed in Kosako et al. (2016) (hereinafter Seto-600m; Fig. 3 and Table 1). The Seto-600m model is in a double-nested configuration based on ROMS with grid spacings of 2 km and 600 m, embedded in the JCOPE2 reanalysis. The surface fluxes are obtained using the bulk formula that has been implemented in the Coupled Ocean/Atmosphere Mesoscale Prediction System (COAMPS; Hodur, 1997). The freshwater discharges from all the major rivers in each model domain are given as monthly climatological freshwater mass point sources based on the Annual Record of Rainfall and Discharge Database issued by the Japan River Association. The Seto-600m model was also carefully validated with observed surface temperature and salinity in Kosako et al. (2016) as well as high-frequency tidal signals in the SIS in Uchiyama et al. (2018b). Other numerical configurations are the same as those of the Seto-2km model, as summarized in Table 1.

It is anticipated that the Seto-2km model would be degraded by design from its higher-resolution counterpart due to the simplified physics and numerical methods for the sake of portability. The point to be confirmed here is whether the Seto-2km is still reasonably precise for WR or not. Fig. 4 shows the comparison of sea-surface variables between the Seto-2km and Seto-600m models averaged over one month in February 2013. The surface temperature agreement is exhibited between the two models, whereas the agreement is moderate for salinity and velocity. The surface salinity of the Seto-2km model is overestimated, especially in the inner-bay areas, because the compact model

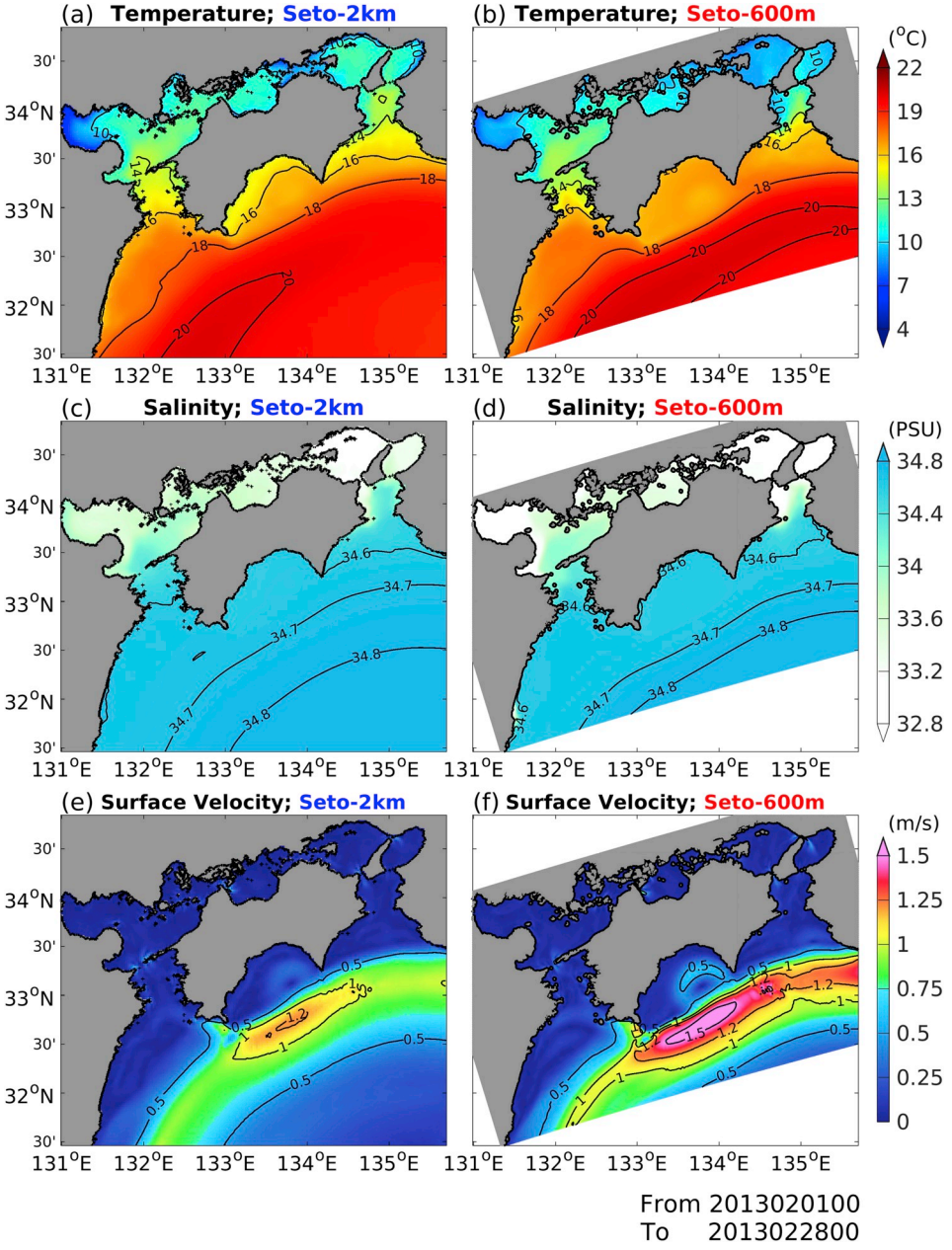

Fig. 4. Spatial maps of temperatures (a and b), salinities (c and d), and velocity magnitudes (e and f) at surface averaged over one month in February 2013. Left panels (a, c, and e) are the Seto-2km model results, while right panels (b, d, and f) are the Seto-600m model results.

does not account for major rivers that results in underestimation of freshwater input to the SIS (Fig. 4c and d). The mean surface velocity distributions of the compact model are almost identical to those of the Seto-600m, despite the modest underestimation in the offshore area around the Kuroshio path, where the highest velocity emerges (Fig. 4e and f). Such velocity intensification is well known to be associated with grid-size refinement, because the frontal structures around the Kuroshio path are better resolved to enhance cross-frontal lateral buoyancy and pressure gradient forces, leading to geostrophic axial acceleration of the Kuroshio. The vertical cross-sectional plots along the A-B line (see Fig. 3 for the location) of the same variables as those in Fig. 4 show that the Seto-2km model successfully reproduces the stratification of temperature and salinity near the Kuroshio front (Fig. 5a and b). In contrast, the streamwise velocity along the Kuroshio has an overall similarity, but with intensified streamwise velocity in the Seto-600m due to the enhanced frontal gradient (Fig. 5e and f). As anticipated, although the model grid resolution and precise forcing are important in ensuring the detailed reproducibility, the Seto-2km model has a reasonable accuracy comparable to the high-resolution model, except for some limited regions such as near river mouths and the Kuroshio path.

Fig. 6 compares the ocean currents of the Seto-2km model and those from *in situ* observation data obtained by the Ministry of Land, Infrastructure, Transport, and Tourism. This data contains current direction and velocity observed by upward-looking ADCPs deployed at the bottoms. The panels show comparisons in three layers, surface, middle, and bottom, at three points shown in Fig. 6a at 12-h intervals for one-month period in February 2013. Root mean square differences (RMSDs) for modeled currents relative to the *in situ* data are calculated as

$$\boldsymbol{RMSD} = \sqrt{\frac{1}{\boldsymbol{n}} \sum_{i=1}^{n} (f_i - y_i)^2}, \tag{5}$$

where n, f, and y are the number of observations, modeled forecast value, and observed value, respectively. At both P1 and P2 in Fig. 6a, the Seto-2km model reproduces currents in the bottom layer better than those in the surface and middle layers (Fig. 6 b-g). The RMSDs at P3 shows that the Seto-2km model estimated the current well at each layer (Fig. 6 h-j). Consequently, even though the Seto-2km model is designed as a compact ocean model, its reproducibility of depth-dependent horizontal current velocity is reasonably well, while we expect significant improvement by using finer resolution and more accurate and sufficient initial condition and forcing datasets.

Fig. 7 shows the result of a tidal harmonic analysis of surface elevations from the Seto-2km model and *in situ* tidal observations at seven tide gauge stations of JMA at Kobe, Wakayama, Komatsushima, Kochi, Matsuyama, Uwajima, and Saiki, shown by the cyan markers in Fig. 3b for a one-month period in February 2013. We show the result for four selected principal tidal constituents (M2, S2, K1, and O1) as scatterplots of amplitudes and phase epochs. It is clearly demonstrated that the amplitudes and phases are reasonably well reproduced by the Seto-2km model with the correlation coefficients of 0.944 and 0.999, respectively. This result assures us that the present Seto-2km model adequately reproduces high-frequency tidal currents prominent in the SIS. From the results demonstrated above, we would conclude that the compact Seto-2km model is exploitable for ship routing problems in the SIS.

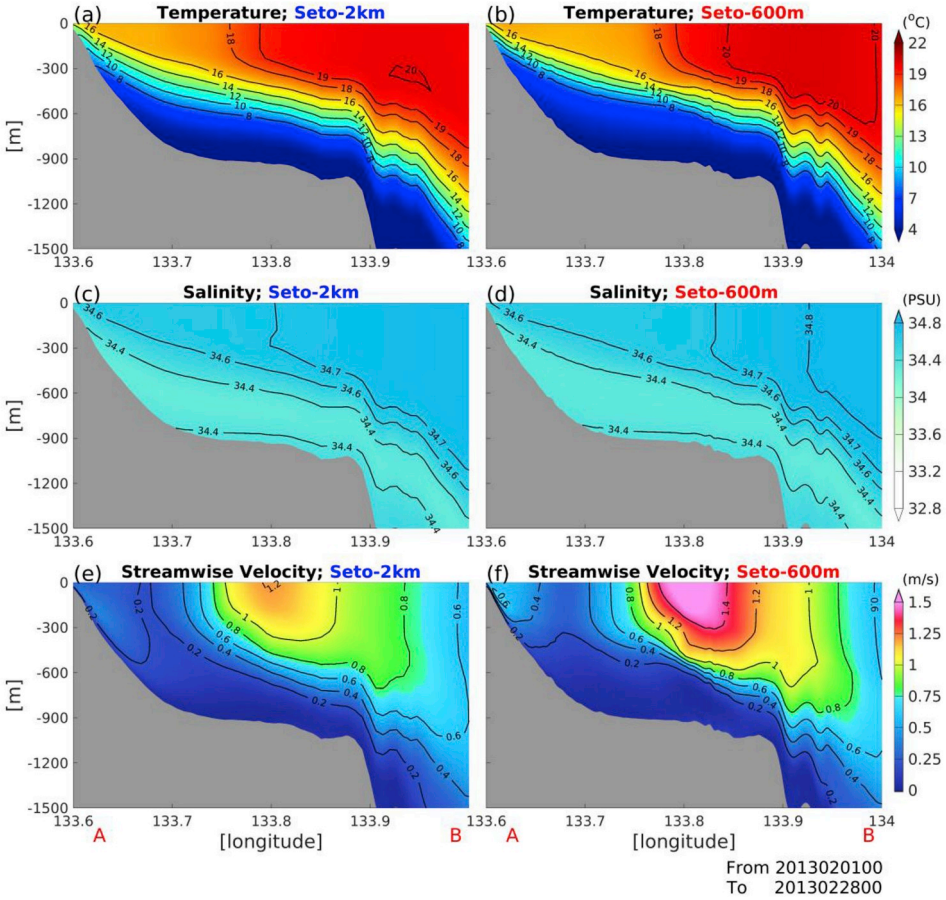

Fig. 5. Cross-sectional plots of temperatures (a and b), salinities (c and d), and streamwise velocities normal to the cross-section (e and f) averaged over one month in February 2013 along the transect A-B shown by the black dotted line in Fig. 3b. Left panels (a, c, and e) are the Seto-2km model results, while right panels (b, d, and f) are the Seto-600m model results.

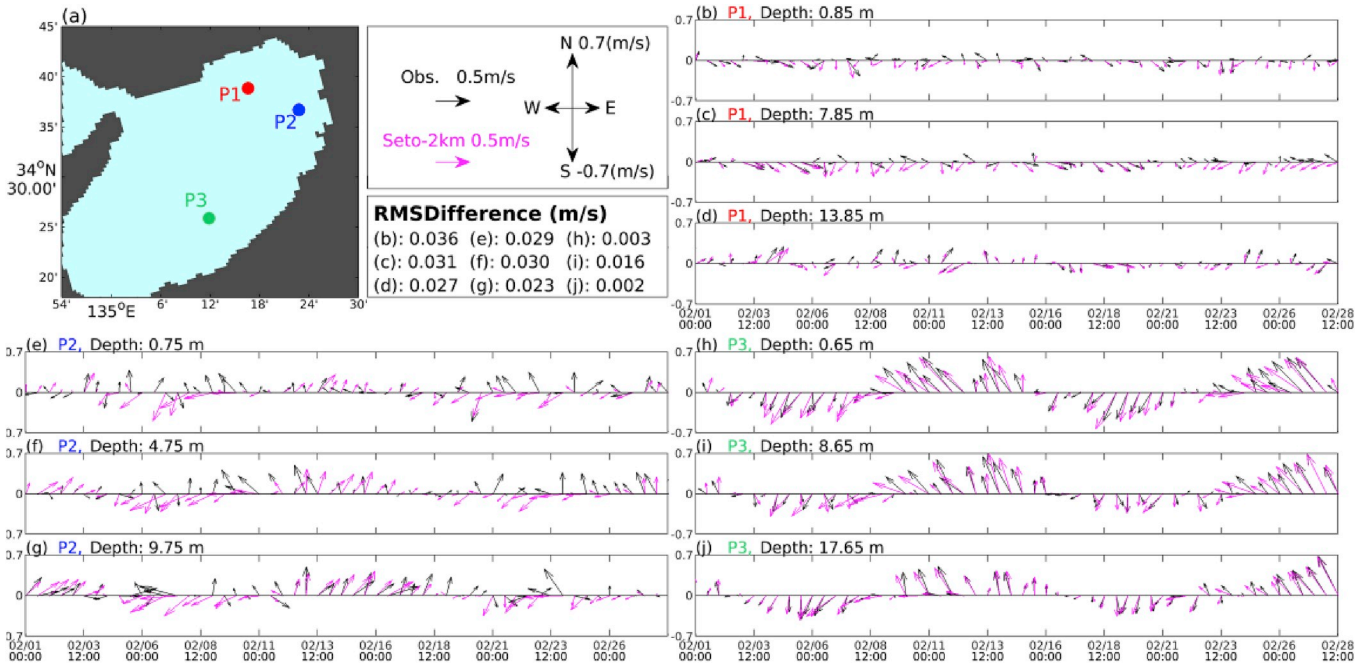

Fig. 6. Spatial map of observation points and time series of current velocity vectors for P1 (b–d), P2 (e–g), and P3 (h–j). Panels (b, e, f), (c, f, i), and (d, g, j) show the data obtained in surface, middle, bottom layer, respectively. The black and magenta vectors show the velocity from observation data and the Seto-2km model, respectively. The observation data is available at 12-h intervals for one month in February 2013. The RMSDs for each point and layer are represented in the top middle box.

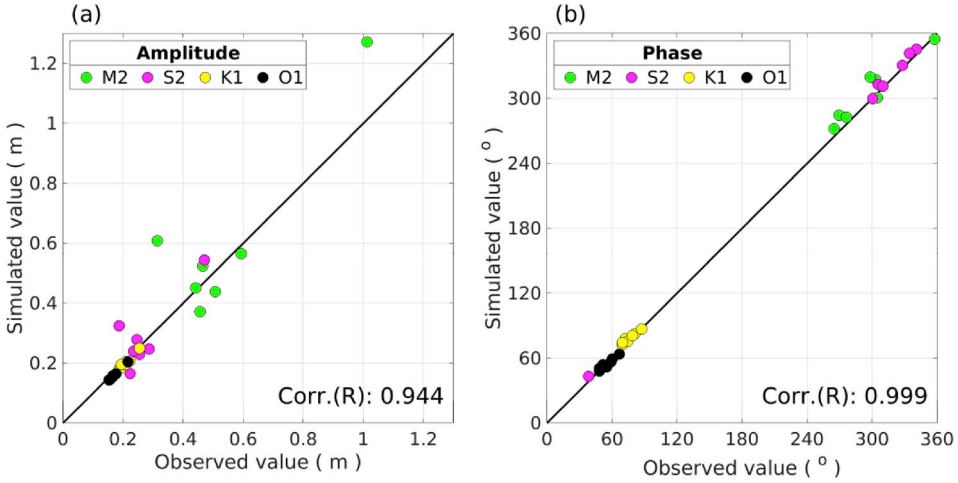

Fig. 7. Scatter plots of four principal tidal constituents (M_2, S_2, K_1, and O_1) derived from the harmonic analysis of hourly surface elevations from Seto-2km model and observations at seven tide gauge locations shown in Fig. 3b. (a) Amplitudes and (b) phase epochs. R in each plot indicates the correlation coefficient.

4. Experiments

4.1. The three new WR methods: a case study for an ocean liner

In this subsection, the optimal routes are evaluated by using the three new routing strategies. A test problem considered here is WR of an ocean liner from Okinawa to Tokyo (Fig. 3b). A key point of this application is how the vessel utilizes the Kuroshio drifting northeastward (Fig. 8). Because the Kuroshio is recognized to be intense enough at up to 3 m/s (~6 kn) to affect a vessel's speed, some previous studies have tried to incorporate the current effects in WR (Chen et al., 2015; Chang et al., 2013). Hourly-averaged oceanic surface currents are provided from the NWPO model, whereas we used the values of surface currents at the departure time that were frozen during the voyage. The rerouting function is also not considered in this experiment for brevity and simplicity. The imposed speed of the vessel is 10 kn unless otherwise stated.

Fig. 8 shows the three optimal routes and associated calculation steps at each of the searched grid points. The black curve in Fig. 8a represents the shortest travel distance route based on the original A-star algorithm. Because this route is simply determined without any oceanic influences, it is merely a straight line connecting the origin and the destination while avoiding islands. We notice that the eastward zonal travel occurs after reaching the coastal area for shorter arcs at higher latitude. By contrast, the shortest travel time route (Fig. 8b) partially utilizes the Kuroshio current flowing mostly parallel to the vessel's track. The vessel does not take a roundabout route on the Kuroshio off Shikoku Island, but rather takes a straight course before it starts using the Kuroshio from the

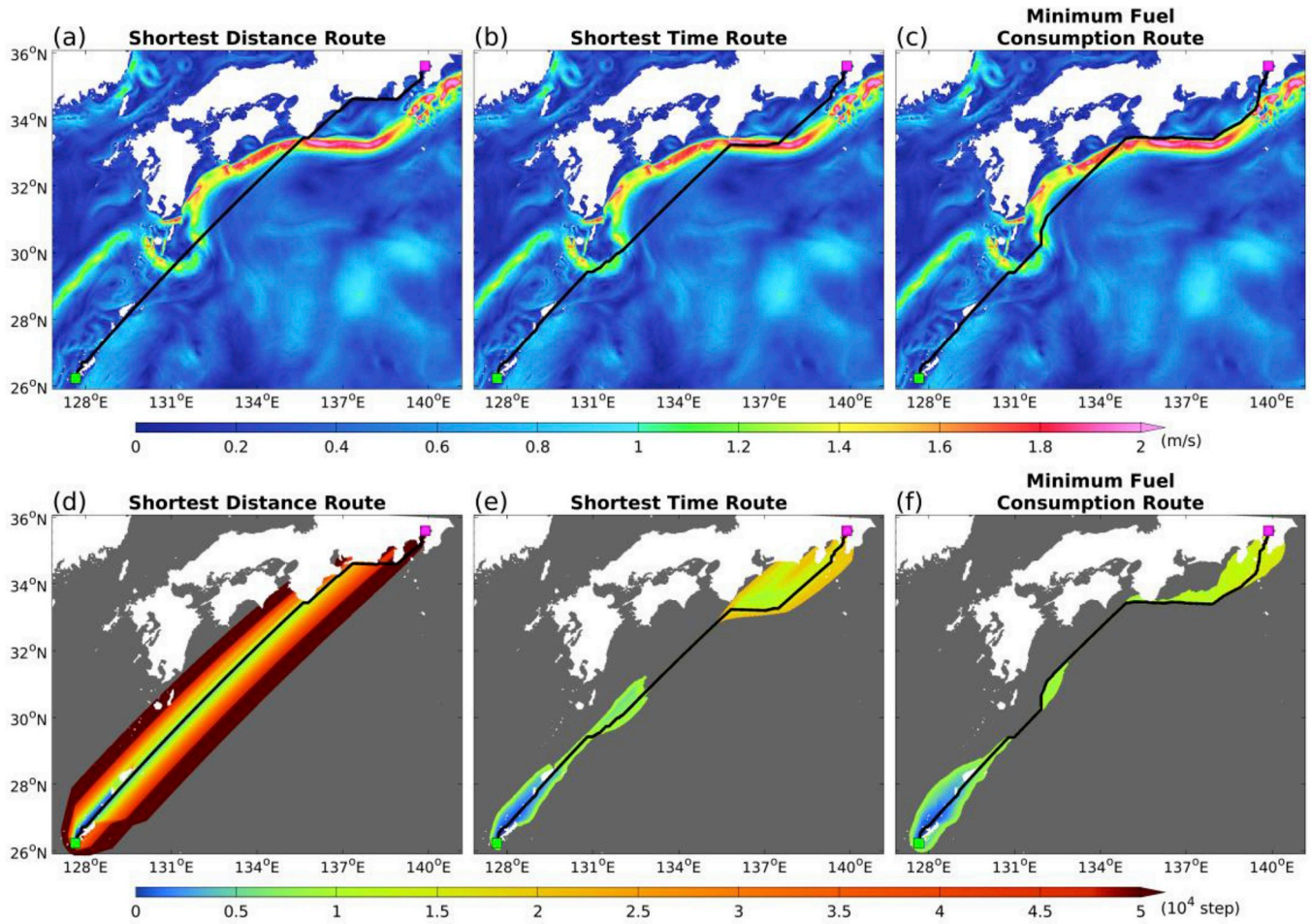

Fig. 8. Optimal routes determined by the newly developed WR algorithms (a, b, and c) and numbers of the searched steps (d, e, and f). Black curves in (a and d), (b and e), and (c and f) are the shortest distance route, shortest time route, and minimum fuel consumption route, respectively. Colors in upper plots indicate the snapshots of the surface velocity magnitude, while those in lower plots are numbers of the searched steps. The green and magenta squares are the origin (Okinawa) and destination (Tokyo), respectively. (For interpretation of the references to color in this figure legend, the reader is referred to the Web version of this article).

Kii Peninsula. On the other hand, the minimal fuel consumption route (Fig. 8c) is quite different from the other two routes. The vessel uses the Kuroshio for a long distance as much as possible to minimize fuel consumption.

The lower panels of Fig. 8 show that the shortest travel time (Fig. 8e) and minimal fuel consumption methods (Fig. 8f) require much fewer searches and thus are computationally more efficient to find the optimal route than the original A-star method (Fig. 8d), even though they account for influences of the Kuroshio in the evaluation of the cost χ. The two weighted A-star searches suggest detours to utilize the Kuroshio following the vessel to reduce χ, whereas the minimal fuel route favors much greater detours. Apparently, the degrees to which the weighted methods recommend utilization of the following currents depend on the ratio of the vessel's speed to the ambient current speed. The Kuroshio current is at 2–3 m/s (4–6 kn) near the ocean surface, which is significant as compared to the vessel's speed set at 10 kn. If the vessel were on the Kuroshio path during its entire voyage, the expected fuel consumption could be minimum on average. However, such a route requires large detours that eventually lead to extra fuel consumption due to longer travel time. The weighted cost functions optimize the balance between these competing influences on the routing purposes. On the other hand, whereas the weighted searches are computationally less costly than the A-star search, the shortest travel time search takes more search steps to finalize the optimization than the minimum fuel search, particularly in the east of the Kii Peninsula. This result illustrates a sensitivity of the optimization to reduce the travel time by considering a balance between the faster vessel's absolute speed due to following the Kuroshio and the longer travel distance due to detours.

The results of the three optimal path findings are summarized in Table 2. Needless to say, the shortest travel distance route is the shortest. In the case of the shortest travel time method, although the distance traveled is longer than the shortest distance route by ~20 km, the algorithm successfully shortens the travel time by approximately 4 h, thanks to the Kuroshio effect. In the case of the minimum fuel consumption method, whereas the traveled distance and time are increased greatly, the fuel consumption is reduced by ~8.4% compared with the shortest distance route. Consequently, it is confirmed that the developed WR algorithms successfully determine the optimal vessel tracks with the three options. It is worth noting that the present method with the weighted cost χ is quite flexible and readily expandable to cases under

Table 2
Traveled time, traveled distance, and fuel efficiency from the results of the three optimal routes shown in Fig. 8. Note that fuel efficiencies are normalized by that of the shortest distance route.

	Traveled Time (min)	Traveled Distance (km)	Fuel Efficiency
Shortest Distance Route	5066.9	1626.8	1.000
Shortest Time Route	4812.7	1647.1	0.969
Minimum Fuel Consumption Route	5232.2	1732.3	0.916

other restrictions such as with retardation of the vessel's speed due to surface waves, winds, and even surrounding traffic.

4.2. Avoidance of a typhoon with the rerouting function

The rerouting and avoidance functions are tested for a case with a typhoon traveling near the vessel track sailing from Tokyo to Okinawa. The same NWPO model used in the preceding application provides the oceanic conditions. An analysis is conducted with the shortest travel time method for the period when Typhoon 201418 (Phanfone) emerges in the domain. Many previous studies have tried to navigate ships in windy and high-wave conditions by estimating the impact of the conditions on the vessel's body and motion (Journée and Meijers, 1980; Shaoze et al., 2016). However, in this subsection, we account for such severe weather conditions as simply as possible to evade complexity associated with interactions between the ship's body and the ocean merely for testing of the implemented avoidance function. The avoidance condition is set with two criteria, viz., wind speed greater than 17.2 m/s and wave height higher than 7.5 m. These weather conditions are provided from the GPV-MSM atmospheric product and the GPV-CWM spectral wave product, both published by the JMA. The nodes that meet either of the two criteria are configured as "obstacles," similar to the land nodes, where the vessel is unnavigable. The time-varying ambient currents are also considered in this experiment. The rerouting is also performed at 1 h intervals to synchronize with the hourly update of the weather and oceanic information.

Fig. 9 shows the snapshots of the migrating typhoon visualized by significant wave height (colors) and wind speed at 10 m above the ocean surface (contours) with the vessel's tracks at intervals of 8 h. The black dotted curve is the shortest travel time route without considering the typhoon, while the blue dotted curves are the predicted shortest time routes sequentially updated with hourly rerouting. The black solid curves are the actual vessel tracks. The optimal vessel track is pronouncedly modified with the updated weather information to successfully avoid encountering the migrating typhoon. Interestingly, the resultant optimal route is on the right side of the typhoon where wind and waves are usually larger than those on the other side in the northern hemisphere. Obviously, this optimal path is affected by the along-coast typhoon track attributable to less severe weather conditions on the right side of the typhoon for the vessel of interest. The vessel navigates towards Okinawa, not only keeping away from the typhoon but also minimizing excess distance traveled to bypass the storm. These results confirm that the present WR algorithm can determine desirable optimal routes with the rerouting and avoidance functionalities.

4.3. Ship routing under strong tidal currents

In this subsection, the Seto-2km compact ocean model is exploited to develop and test a quasi-standalone WR system suitable for regional ship navigation in estuaries, bays, and harbors. As argued in Section 3, this model is sufficiently capable of running on laptop computers, tablets, and smartphones on the ship while maintaining reasonable accuracy. Therefore, our motivation to employ such a compact model totally differs from that in the preceding subsections, where the high-resolution oceanic downscaling products originally designed for research purposes were used for precise evaluation of the proposed algorithms.

The SIS is characterized by complex topography that forms a typical basin-strait system (Fig. 3), where strong semi-diurnal tidal currents

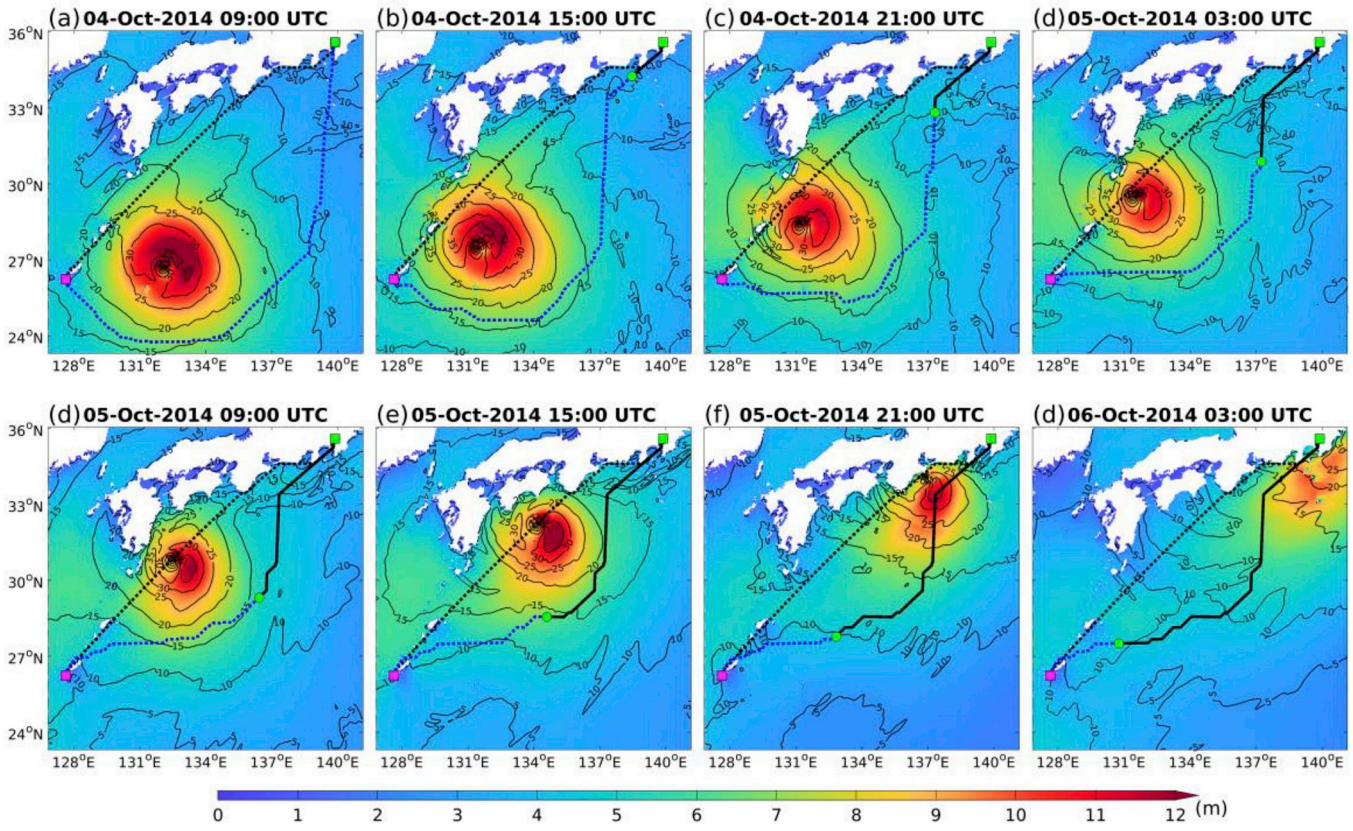

Fig. 9. Snapshots of the migrating typhoon and optimal routes with the rerouting function at intervals of 8 h. Colors indicate significant wave heights from GPV-CWM, and contours are surface wind speeds from GPV-MSM. The dotted black curves are the shortest travel time routes without considering the typhoon, while the dotted blue curves are the predicted shortest time routes sequentially updated with hourly rerouting. The solid black curves are the actual vessel tracks. The green and magenta squares are the origin (Tokyo) and destination (Okinawa), respectively. Green circle is the position of the vessel at the labeled time. (For interpretation of the references to color in this figure legend, the reader is referred to the Web version of this article).

develop near topographies (e.g., Uchiyama et al., 2018b; Zhang et al., 2019). We intend to find the optimal southwestward routes from Osaka to Kagawa, which requires passing a narrow tidal strait where tidal currents are quite energetic. Because tidal currents fluctuate largely at the semi-diurnal period in the area, travel time and fuel efficiency are affected by their direction and intensity that depend on tidal phase and thus on the departure time.

Fig. 10 shows the optimal routes from Osaka to Kagawa with the shortest travel time method for the ship operated at 10 kn leaving Osaka every 6 h from 0:00 UTC on February 22, 2013. The color represents the horizontal velocity magnitude averaged over the 6 h after each departure. The vectors correspond to the direction and speed of the time-averaged tidal currents. Overall, the determined shortest travel time routes are similar to each other among all the cases. The present WR system suggests passing through the northern strait with rather straight routes from the origin to the strait and from the strait to the destination. The most striking differences associated with the tidal phase are confirmed by comparing two cases, in which the ship departs at 12:00 and 18:00 on February 22 in 2013 (Fig. 10c and d). As labeled in Fig. 10, although the estimated routes, travel distances, and durations are approximately the same, the difference of fuel efficiency is 14.5% for these two cases. Fig. 11 shows the time series of the fuel efficiency according to the departure times shown on the abscissa, normalized by that with the least efficiency. The estimated fuel efficiency with different departure times varies at a ~12-h period. We found that the overall fuel efficiency depends on the condition of the tidal currents at the northern strait, rather than on the departure time. Apparently, this is caused by the predominance of the semi-diurnal tidal variability in the SIS. For instance, Fig. 10c clearly demonstrates that strong eastward tidal currents occur at the strait, where the narrow channel topography intensifies tidal currents opposing the westward traveling vessel, resulting in deceleration of the vessel. In turn, if the vessel leaves the origin at 18:00 (Fig. 10d), it approaches the strait at ~20:00, when the tidal currents are headed westward to accelerate the vessel. From these

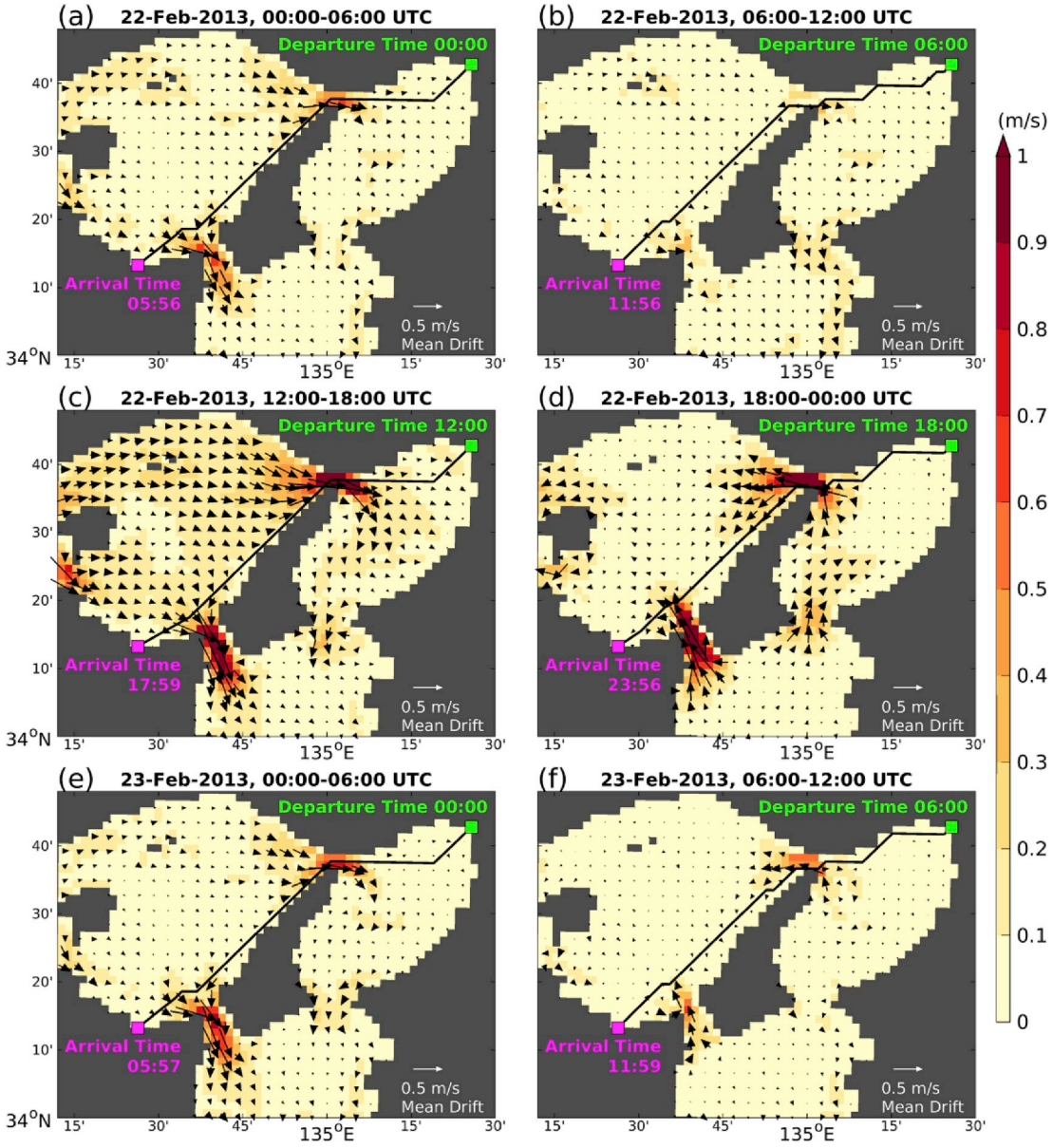

Fig. 10. Shortest time routes from Osaka (the origin, green square marks) to Kagawa (the destination, magenta square marks) with different departure times occurring every 6 h from 0:00 UTC on February 22, 2013. Colors indicate the surface velocity magnitudes averaged over 6 h after each departure. The black vectors are superposed to show the subsampled time-averaged surface current velocity. (For interpretation of the references to color in this figure legend, the reader is referred to the Web version of this article).

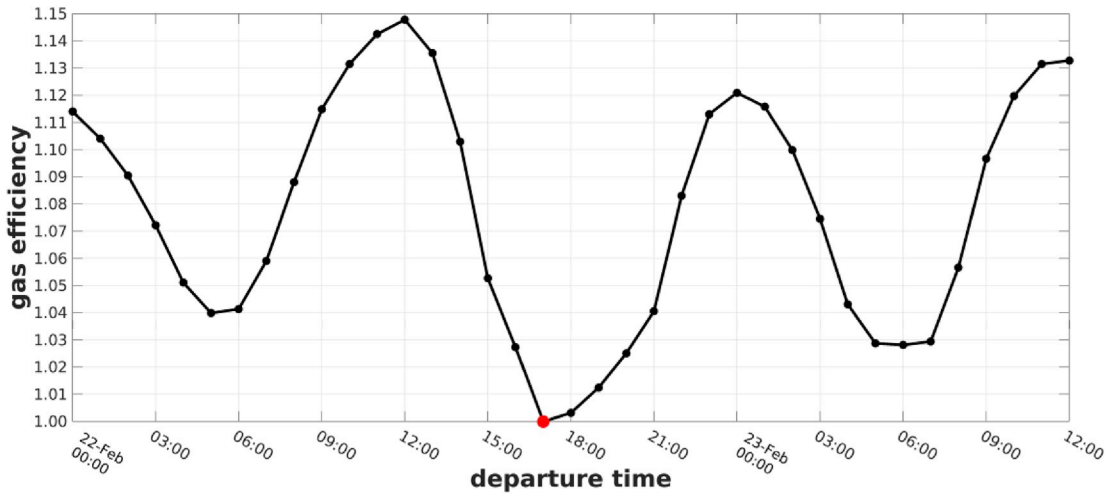

Fig. 11. Fuel efficiencies for labeled departure times in the abscissa, starting at 0:00 UTC on February 22, 2013. The fuel efficiency is relative to that at 17:00 UTC (red circle). (For interpretation of the references to color in this figure legend, the reader is referred to the Web version of this article).

results, the direction of the semi-diurnal tidal currents in such a small estuary has a pronounced impact on vessel speed, leading to substantial alteration of fuel efficiency.

5. Conclusions

This study aimed to develop a weather routing (WR) system for vessel navigation based on the A-star algorithm. Building upon the heuristics introduced to reduce computational cost as compared to that of the widely used Dijkstra's algorithm, the cost function was additionally modified to account for oceanic and atmospheric conditions around the vessel of interest. Three options were implemented to search for the optimal paths with the shortest travel time, minimal fuel consumption, and shortest travel distance. In addition, we introduced a rerouting function that recalculates and updates the optimal route recursively whenever the route should be reconsidered with updated oceanic and weather information. An avoidance function to exclude specific nodes from the search was also incorporated into the WR system by setting thresholds according to oceanic and weather conditions. The ocean liner examples along the northeastward drifting Kuroshio current off Japan with and without a migrating typhoon were chosen to test the developed WR system and to confirm the expected functionalities.

Furthermore, a compact regional ocean circulation model, which is sufficiently accurate and executable on typical laptop PCs, was configured for a vessel-borne WR system. This compact model was successfully applied to evaluate the optimal vessel paths in the SIS, where high-frequency tidal currents modified by complex topographies are significant enough to alter the vessel's absolute speed, to which fuel efficiency is eventually attributed to a remarkable extent. In this study, our purpose was accomplished by using simple datasets to design the compact ocean model. For further applying this method to the practical implementation of WR systems in the Japan's neighboring seas in the future, the compact model will need to be operational and also coupled with atmospheric models. In such a case, the compact model would become more complicated and time-consuming, because forecasts of winds, waves, and currents for several days up front are necessary. In other words, more accurate and sophisticated WR system will be realized with higher-performance PC and more frequent data updates.

The developed WR system is quite general, computationally very low cost, and universally applicable to any vessel navigation scenarios, not only in the open ocean but also in estuaries and harbors with complex topographies. Although we mostly examined the effects of the ambient surface currents, the proposed weighted-cost function based on the A-star algorithm has substantial flexibility and expandability to account for arbitrary oceanic and weather conditions around the vessel. Possible modifications are to be made by adjusting the weight defined as a function of the vessel's speed. For instance, given detailed wave or wind conditions around the vessel, the traveling speed may be altered accordingly, which in turn influences the effective inter-node distance equivalent to the weighted cost. The challenge towards an integrated vessel-borne WR system with a compact ocean model is also a unique undertaking of this study. Such a system allows us tremendous flexibility in utility of the marine WR, even though data retrieval is impossible or largely limited if the vessel is out of radio range under certain circumstances, including cases of severe natural disasters.

Acknowledgments

This study was financially supported by the Japan Society for the Promotion of Science (JSPS) Grants-in-Aid for Scientific Research 15KK0207 and 18H03798 at Kobe University. We also appreciate Yota Suzue (CTI Engineering Co., Ltd.), Hiroaki Tada (Nippon Koei Co. Ltd), and Yasumasa Miyazawa (Japan Agency for Marine-Earth Science and Technology) for their help in the development of the ROMS models embedded in the assimilative Japan Coastal Ocean Predictability Experiments (JCOPE2) oceanic reanalysis that was used in the present study.

References

Andersson, A., 2015. Multi-objective Optimisation of Ship Routes. Master's thesis. Chalmers University of Technology, Göteborg, Sweden.

Bialystocki, N., Konovessis, D., 2016. On the estimation of ship's fuel consumption and speed curve: a statistical approach. J. Ocean Eng. Sci. 1 (2), 157–166. https://doi.org/10.1016/j.joes.2016.02.001.

Bouman, E.A., Lindstad, E., Rialland, A.I., Strømman, A.H., 2017. State-of-the-art technologies, measures, and potential for reducing GHG emissions from shipping – a review. Transp. Res. D Transp. Environ. 52 (A), 408–421. https://doi.org/10.1016/j.trd.2017.03.022.

Buhaug, Ø., Corbett, J.J., Endresen, Ø., Eyring, V., Faber, J., Hanayama, S., Lee, D.S., Lee, D., Lindstad, H., Markowska, A.Z., Mjelde, A., Nelissen, D., Nilsen, J., Pålsson, C., Winebrake, J.J., Wu, W.Q., Yoshida, K., 2009. Second IMO GHG Study 2009. International Maritime Organization, London, UK.

Calvert, S., Deakins, E., Motte, R., 1991. A dynamic system for fuel optimisation trans-ocean. J. Navig. 44 (2), 233–265. https://doi.org/10.1017/S0373463300009978.

Chen, C., Shiotani, S., Sasa, K., 2013. Numerical ship navigation based on weather and ocean simulation. Ocean Eng. 69, 44–53. https://doi.org/10.1016/j.oceaneng.2013.05.019.

Chen, C., Shiotani, S., Sasa, K., 2015. Effect of ocean currents on ship navigation in the east China sea. Ocean Eng. 104, 283–293. https://doi.org/10.1016/j.oceaneng.2015.04.062.

Chang, Y.C., Tseng, R.S., Chen, G.Y., Chu, P.C., Shen, Y.T., 2013. Ship routing utilizing strong ocean currents. J. Navig. 66, 825–835. https://doi.org/10.1017/S0373463313000441.

De Wit, C., 1990. Proposal for low cost ocean weather routing. J. Navig. 43 (3), 428–439. https://doi.org/10.1017/S0373463300014053.
Dijkstra, E.W., 1959. A note on two problems in connexion with graphs. Numer. Math. 1 (1), 269–271. https://doi.org/10.1007/BF01386390.
Efentakis, A., Pfoser, D., Voisard, A., 2011. Efficient data management in support of shortest-path computation. In: Proc. The 4th ACM SIGSPATIAL International Workshop on Computational Transportation Science. ACM Press, pp. 28–33. https://doi.org/10.1145/2068984.2068990.
Egbert, G.D., Erofeeva, S.Y., 2002. Efficient inverse modeling of barotropic ocean tides. J. Atmos. Ocean. Technol. 19 (2), 183–204.
Egbert, G.D., Bennett, A.F., Foreman, M.G.G., 1994. TOPEX/POSEIDON tides estimated using a global inverse model. J. Geophys. Res. 99 (C12), 24821–24852. https://doi.org/10.1029/94JC01894.
Hagiwara, H., 1989. Weather Routing of Sail-Assisted Motor Vessels. Ph. D. thesis. Delft University of Technology, The Netherlands.
Hodur, R.M., 1997. The naval research laboratory's coupled ocean/atmosphere mesoscale prediction system (COAMPS). Mon. Weather Rev. 125, 1414–1430.
Hart, P.E., Nilsson, N.J., Raphael, B., 1968. A formal basis for the heuristic determination of minimum cost paths. IEEE Trans. Syst. Sci. Cybern. 4 (2), 100–107. https://doi.org/10.1109/TSSC.1968.300136.
Journée, J.M.J., Meijers, J.H.C., 1980. Ship routing for optimum performance: Part I Prediction of speed and power of a ship in a seaway. Trans. IME 12–21.
Jung, J.S., Rhyu, K.S., 1999. A study on the optimal navigation route decision using A* algorithm. J. Korean Inst. Off. Autom. 4 (1), 38–46.
Kim, K., Lee, K.M., 2018. Dynamic programming-based vessel speed adjustment for energy saving and emission reduction. Energies 11 (5), 1273. https://doi.org/10.3390/en11051273.
Kosako, T., Uchiyama, Y., Mitarai, S., 2016. A multi-year analysis on circulation and associated larval transport in the Seto Inland Sea, Japan. J. Jpn Soc. Civil Eng. Ser. B2 72 (2), 1273–1278 (in Japanese with English abstract).
Kosmas, O.T., Vlachos, D.S., 2012. Simulated annealing for optimal ship routing. Comput. Oper. Res. 39 (3), 576–581. https://doi.org/10.1016/j.cor.2011.05.010.
Lu, R., Turan, O., Boulougouris, E., Banks, C., Incecik, A., 2015. A semi-empirical ship operational performance prediction model for voyage optimization towards energy efficient shipping. Ocean Eng. 110 (B), 18–28. https://doi.org/10.1016/j.oceaneng.2015.07.042.
Marchesiello, P., McWilliams, J.C., Shchepetkin, A.F., 2003. Equilibrium structure and dynamics of the California current system. J. Phys. Oceanogr. 33, 753–783.
Miyazawa, Y., Zhang, R., Guo, X., Tamura, H., Ambe, D., Lee, J., Okuno, A., Yoshinari, H., Setou, T., Komatsu, K., 2009. Water mass variability in the Western North Pacific detected in 15-year eddy resolving ocean reanalysis. J. Oceanogr. 65 (6), 737–756. https://doi.org/10.1007/s10872-009-0063-3.
Papanikolaou, A., Zaraphonitis, G., Bitner-Gregersen, E., Shigunov, V., El Moctar, O., Guedes Soares, C., Reddy, D.N., Sprenger, F., 2016. Energy efficient safe SHip OPERAtion (SHOPERA). Transp. Res. Procedia. 14, 820–829. https://doi.org/10.1016/j.trpro.2016.05.030.
Roh, M.I., 2013. Determination of an economical shipping route considering the effects of sea state for lower fuel consumption. Int. J. Nav. Archit. Ocean Eng. 5 (2), 246–262. https://doi.org/10.3744/JNAOE.2013.5.2.246.
Sen, D., Padhy, C., 2010. Development of a ship weather-routing algorithm for specific application in North Indian Ocean Region. Int. Conf. Mar. Technol. (MARTEC) 2010, 21–27.
Shaoze, L., Ning, M., Hirakawa, Y., 2016. Evaluation of resistance increase and speed loss of a ship in wind and waves. J. Ocean Eng. Sci. 1 (3), 212–218. https://doi.org/10.1016/j.joes.2016.04.001.
Shchepetkin, A.F., McWilliams, J.C., 2005. The regional ocean modeling system (ROMS): a split-explicit, free-surface, topography-following-coordinate oceanic model. Ocean Model. 9 (4), 347–404. https://doi.org/10.1016/j.ocemod.2004.08.002.
Shchepetkin, A.F., McWilliams, J.C., 2008. Computational kernel algorithms for fine-scale, multiprocess, longtime oceanic simulations. Handb. Numer. Anal. 14, 119–181. https://doi.org/10.1016/S1570-8659(08)01202-0.
Smierzchalski, R., Michalewicz, Z., 2000. Modeling of a ship trajectory in collision situations at sea by evolutionary algorithm. IEEE Trans. Evol. Comput. 4 (3), 227–241. https://doi.org/10.1109/4235.873234.
Szlapczynska, J., 2007. Multiobjective approach to weather routing. Trans. Nav. Int. J. Mar. Navig. Saf. Sea Transp. 1 (3), 273–278.
Tada, H., Uchiyama, Y., Masunaga, E., 2018. Impacts of two super typhoons on the Kuroshio and marginal seas on the Pacific coast of Japan. Deep. Res. Part I 132, 80–93. https://doi.org/10.1016/j.dsr.2017.12.007.
Trodden, D.G., Murphy, A.J., Pazouki, K., Sargeant, J., 2015. Fuel usage data analysis for efficient shipping operations. Ocean Eng. 110 (B), 75–84. https://doi.org/10.1016/j.oceaneng.2015.09.028.
Tsou, M.-C., Cheng, H.-C., 2013. An ant colony algorithm for efficient ship routing. Pol. Marit. Res. 20 (3), 28–38. https://doi.org/10.2478/pomr-2013-0032.
Uchiyama, Y., Kanki, R., Takano, A., Yamazaki, H., Miyazawa, Y., 2018. Mesoscale reproducibility in regional ocean modeling with a 3-D stratification estimate based on Aviso-Argo data. Atmos.-Ocean 56 (4), 212–229. https://doi.org/10.1080/07055900.2017.1399858.
Uchiyama, Y., Zhang, X., Suzue, Y., Kosako, T., Miyazawa, Y., Nakayama, A., 2018. Residual effects of treated effluent diversion on a seaweed farm in a tidal strait using a multi-nested high-resolution 3-D circulation-dispersal model. Mar. Pollut. Bull. 130, 40–54. https://doi.org/10.1016/j.marpolbul.2018.03.007.
Walther, L., Rizvanolli, A., Wendebourg, M., Jahn, C., 2016. Modeling and optimization algorithms in ship weather routing. Int. J. e-Navigation Marit. Econ. 4, 31–45. https://doi.org/10.1016/j.enavi.2016.06.004.
Wei, S., Zhou, P., 2012. Development of a 3D dynamic programming method for weather routing. Trans. Nav. Int. J. Mar. Navig. Saf. Sea Transp. 6 (1), 79–85.
Zhang, X., Uchiyama, Y., Nakayama, A., 2019. On relaxation of the influences of treated sewage effluent on an adjacent seaweed farm in a tidal strait. Mar. Pollut. Bull. 144, 265–274. https://doi.org/10.1016/j.marpolbul.2019.04.050.